Journal of Materials and Environmental Sciences
ISSN : 2028-2508

JMES, 2017 Volume 8, Issue 11, Page XX-XX

http://www.jmaterenvironsci.com

Mild Steel Corrosion Mitigation by (2Z)-(4-Chlorobenzylidene)-2*H*-[1,4]-Benzothiazin-3(4*H*)-one in 1.0 M HCl: Electrochemical and DFT Evaluation

G. Aziate[1], H. Elmsellem[2*], N.K. Sebbar[3], Y. El Ouadi[2], M. Ellouz[1], M. Rassam[5], S. El Hajjaji[1], E. M. Essassi[3,4], I. Abdel-Rahman[6] and R. Benkaddour[2]

[1]*Laboratory of Spectroscopy, Molecular Modeling, Materials and Environment (LS3ME), Mohammed V University, Faculty of Science Rabat, Ibn Battouta street, PB 1014 Agdal. Morocco.*

[2]*Laboratoire de chimie analytique appliquée, matériaux et environnement (LC2AME), Faculté des Sciences, B.P. 717, 60000 Oujda, Morocco.*

[3]*Laboratoire de Chimie Organique Hétérocyclique, URAC 21, Pôle de Compétences Pharmacochimie, Mohammed V University Rabat, Faculté des Sciences, Av. Ibn Battouta, BP 1014 Rabat, Morocco.*

[4]*Moroccan Foundation for Advanced Science, Innovation and Research (MASCIR), Rabat Design Center, Rue Mohamed Al Jazouli, Madinat El Irfane, Rabat, Morocco.*

[5]*Laboratoire de Procédés, Matériaux et Enérigie Solaire (PROMES-CNRS), Université de Perpignan Via Domitia, 52, Avenue Paul Alduy, 66000, Perpignan, France.*

[6]*Department of Chemistry, College of Sciences, University of Sharjah, PO Box: 27272, UAE.*

Received 28 Mar 2017,
Revised 27 May 2017,
Accepted 31 May 2017

Keywords
- ✓ Mild steel*;*
- ✓ Corrosion*;*
- ✓ EIS *;*
- ✓ benzothiazin-3(4H)-one*;*
- ✓ DFT*;*
- ✓ Fukui function *;*
- ✓ Electrochemical.

H. Elmsellem
h.elmsellem@gmail.com
Phone: (+212)670923431

Abstract

Adsorption of (2Z)-(4-chlorobenzylidene)-2H-[1,4]-benzothiazin-3(4H)-one (**G3**) on mild steel surface in 1.0 M HCl solution and its corrosion inhibition properties have been studied by the following techniques: potentiodynamic polarization, electrochemical impedance spectroscopy (EIS), weight loss measurements and quantum chemical calculations. Potentiodynamic polarization measurements showed that 1,4-benzothiazine derivative acts as a cathodic type inhibitor. The degree of surface coverage was determined using weight loss measurements. It was found that adsorption process of the studied inhibitor on mild steel surface obeys Langmuir adsorption isotherm. Quantum chemical calculations well support the experimental results.

1. Introduction

Corrosion inhibition of materials has been the focus of research for centuries and in many cases well analyzed and understood [1-3]. Corrosion of materials has continued to receive interest in the technological world. In the field of corrosion inhibition, scientists are persistent in seeking better and more efficient ways of combating the corrosion of metals. Addition of corrosion inhibitors to the corrosion environment with respect to the other methods of corrosion inhibition employed [4]. Nitrogen-containing heterocyclic are undoubtedly one of the most important targets in organic chemistry. They are widely distributed in natural products and in pharmaceutical agents and numerous studies for their chemistry and synthesis have been reported. Benzothiazines and their analogues have extensively been studied in different areas of chemistry including the pharmaceuticals [5–9] and biological applications. These compounds are found to have potent anti-inflammatory [10-11], analgesic [12], anti-pyretic [13], anti-microbial [14] and anti-oxidant [15].

A slight change in the substitution pattern in the derivatives of benzothiazine nucleus causes distinguishable difference in their biological activities [16–17].The use of corrosion inhibitors constitutes one of the most economical ways to mitigate the corrosion rate and to protect metal surface against corrosion and preserve industrial facilities, especially in acidic media. The inhibition of steel in acid solutions by different types of organic inhibitors had been extensively studied. Among these compounds, the use of environmentally

acceptable inhibitors such as the N-heterocyclic organic compounds (triazoles, oxadiazoles, thiadiazoles, pyrazoles, benzothiazine, pyridines … etc.) [18-20].

The present study aimed to test the effect of a new synthesized compound named (2Z)-(4-chlorobenzylidene)-2H-[1,4]-benzothiazin-3(4H)-one (**G3**) and shown in Figure 1, on the corrosion of mild steel in **1.0 M** hydrochloric acid solution,

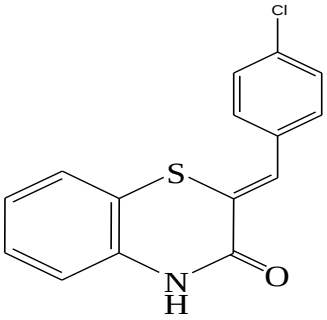

Figure 1. Chemical structure of (2Z)-(4-chlorobenzylidene)-2*H*-[1,4]-benzothiazin-3(4*H*)-one (**G3**).

2. Experimental

2.1. Synthesis of inhibitor

A solution of 3,4-dihydro-2*H*-1,4-benzothiazin-3-one (2.78 mmol) in 10 ml of DMF was mixed with an excess amounts of sodium methoxide and 4-chlorobenzaldehyde (6.52 mmol) and the mixture was refluxed with stirring for 48 hrs. The salts were removed by filtration and the filtrate was concentrated under reduced pressure. The residue was chromatographed on silica gel column and the compound G3 was recrystallized using hexane as a solvent (Scheme 1**)**.

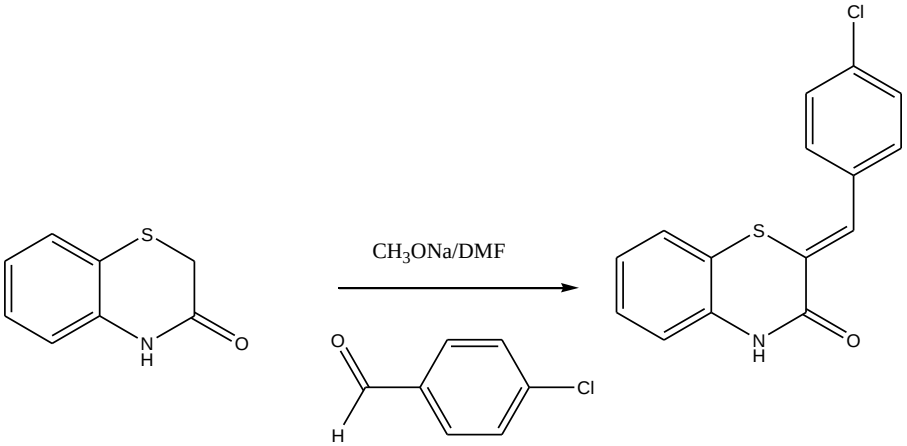

Scheme 1. Synthesis of (2Z)-(4-chlorobenzylidene)-2*H*-[1,4]-benzothiazin-3(4*H*)-one (**G3**).

The below analytical and spectroscopic data are conforming the structure of the synthesized compound G3.

(G3): Yield: 82 %; mp: 391 **K; NMR^{1}H (DMSO-d$_6$) δ ppm:** 6.94-7.56 (m, 8H, H_{ar}); 7.76 (s, 1H; =CH-C_6H_5); 11.01 (s, 1H; NH); **NMR^{13}C (DMSO-d$_6$) δ ppm**: 117.4, 123.6, 124.9, 126.7, 128.5, 129.3, 130.3, 131.2 (CH_{ar}); 115.4, 121.8, 122.6, 134.2, 134.5 (Cq), 159.1 (C=O).

2.2. Materials and solutions

2.2.1. Experimental procedure

For the weight loss technique, the chemical composition of the investigated mild steel in (wt. %) is as follows: 0.2 % C, 0.38 % Si, 0.09 % P, 0.01 % Al, 0.05 % Mn, 0.05 % S and 99.22 % Fe. The samples of mild steel were mechanically polished with different emery paper SiC (grade 120, 1200) before each experiment, washed with distilled water and acetone and finally dried in air at room temperature.

The aggressive 1.0 M HCl solution was prepared by diluting the Analytical Grade 37% HCl with bidistilled water. The concentration range of the inhibitor G3 was in the range (10^{-3} to 10^{-6}) M. Gravimetric measurements were carried out in a double walled glass cell equipped with a thermostat-cooling condenser. The initial weight of each specimen was measured using an analytical balance and then the specimens were immersed in 1.0 M HCl solutions without and with different concentrations of the G3 inhibitor for 6 hrs. at 308K. Finally, the specimens were washed and reweighed.
The average weight loss was obtained. The corrosion rate (v) is calculated using the following equation:

$$v = \frac{w}{S.t} \quad \textbf{(1)}$$

Where, W is the average weight loss, S the total specimen surface area, and t is the immersion time. With the corrosion rate calculated, the inhibition efficiency (Ew) is determined as follows:

$$\text{Ew } \% = \frac{\text{V0}-\text{V}}{\text{V0}} \text{ X } 100 \quad \textbf{(2)}$$

Where, V_0 and V are the values of corrosion rate without and with inhibitor, respectively.
Electrochemical measurements were conducted using a potentiostat PGZ100 piloted by Voltamaster software and connected to a conventional three electrode cylindrical Pyrex glass cell. The working electrode (WE) had the form of a disc cut from the steel sheet, a saturated calomel electrode (SCE) was used as reference and a platinum plate was used as counter electrode. Before all runs, the potential was stabilized at free potential during 30 minutes, the polarization measurements were performed by applying a controlled potential scan automatically from –800 to –200 mV at a scan rate of 1 mV/s [21, 22]. A 10 mV peak to peak sine wave over a frequency range extending from 10 mHz to 100 MHz was used for the impedance measurements. Inhibition efficiency (Ep%) is determined using the following equation:

$$\text{Ep}\% = \frac{\text{icorr (0)}-\text{icorr (inh)}}{\text{icorr (0)}} \text{ x } 100 \quad \textbf{(3)}$$

Where, $i_{corr(0)}$ and $icorr_{(inh)}$ represent corrosion current density values without and with inhibitor, respectively.
The impedance tests have been performed in non-aerated solutions and the impedance diagrams are given in the Nyquist representation. All electrochemical studies were made at 308 K for an immersion time of 1/2 h, with different concentrations of the inhibitor G3.

Inhibition efficiency (E_R%) is estimated using the below relation, equation 4.

$$E_R\% = \frac{\text{Rt(inh)}-\text{Rt(0)}}{\text{Rt(inh)}} \text{x} 100 \quad \textbf{(4)}$$

Where, Rt(0) and Rt(inh) are the charge transfer resistance values in the absence and presence of inhibitor, respectively

2.3. Theory and computational details

Quantum chemical calculations are used to correlate experimental data for inhibitors obtained from different techniques (viz., electrochemical and weight loss) and their structural and electronic properties. According to Koop man's theorem [23], E_{HOMO} and E_{LUMO} of the inhibitor molecule are related to the ionization potential (I) and the electron affinity (A), respectively. The ionization potential and the electron affinity are defined as $I = -E_{HOMO}$ and $A = -E_{LUMO}$, respectively. Then absolute electronegativity (χ) and global hardness (η) of the inhibitor molecule are approximated as follows [24]:

$$\chi = \frac{I+A}{2}, \ \chi = -\frac{1}{2}(E_{HOMO} + E_{LUMO}) \quad \textbf{(5)}$$

$$\eta = \frac{I-A}{2}, \ \eta = -\frac{1}{2}(E_{HOMO} - E_{LUMO}) \quad \textbf{(6)}$$

Where $I = -E_{HOMO}$ and $A = -E_{LUMO}$ are the ionization potential and electron affinity respectively.
The fraction of transferred electrons ΔN was calculated according to Pearson theory [23]. This parameter evaluates the electronic flow in a reaction of two systems with different electronegativities, in particular case; a metallic surface (Fe) and an inhibitor molecule. ΔN is given as follows:

$$\Delta N = \frac{\chi_{Fe}-\chi_{inh}}{2(\eta_{Fe}+\eta_{inh})} \quad \textbf{(7)}$$

Where χ_{Fe}andχ_{inh} denote the absolute electronegativity of an iron atom (Fe) and the inhibitor molecule, respectively; η_{Fe} and ηinh denote the absolute hardness of Fe atom and the inhibitor molecule, respectively. In order to apply the eq.7 in the present study, a theoretical value for the electronegativity of bulk iron was used χ_{Fe} = 7 eV and a global hardness of η_{Fe} = 0, by assuming that for a metallic bulk I = A because they are softer than the neutral metallic atoms [25]. The electrophilicity has been introduced by Sastri *et. Al.* [24], is a descriptor of reactivity that allows a quantitative classification of the global electrophilic nature of a compound within a relative scale. They have proposed the ω as a measure of energy lowering owing to maximal electron flow between donor and acceptor and ω is defined as follows:

$$\omega = \frac{\chi^2}{2\eta} \qquad \textbf{(8)}$$

The Softness σ is defined as the inverse of the η [26] and represented in equation 9.

$$\sigma = \frac{1}{\eta} \qquad \textbf{(9)}$$

Using left and right derivatives with respect to the number of electrons, electrophilic and nucleophilic Fukui functions for a site k in a molecule can be defined [26]:

$$f_k^+ = P_k\ (N+1) - P_k\ (N)\ for\ nucleophilic\ attack \qquad (\mathbf{10})$$

$$f_k^- = P_k\ (N) - P_k\ (N-1)\ for\ electrophilic\ attack \qquad (\mathbf{11})$$

$$f_k^+ = [P_k\ (N+1) - P_k\ (N-1)]/2\ for\ radical\ attack \qquad (\mathbf{12})$$

3. Results and Discussion

3.1. Weight loss measurement

The relationships between inhibition efficiency (E%) and the corrosion rate (v) with the inhibitor G3 concentration are shown in Figure 2. Apparently, Figure 2 shows that E% increases with the increase in inhibitor concentration. This is due to the fact that with the increase of inhibitor concentration, adsorption and surface coverage increases and thus the surface protected from the corrosive medium [30]. It is clearly observed from this below figure, that the inhibition efficiency increased, but the corrosion rate decreased with the increase in the concentration of the G3 inhibitor from 10^{-6} to 10^{-3}M.

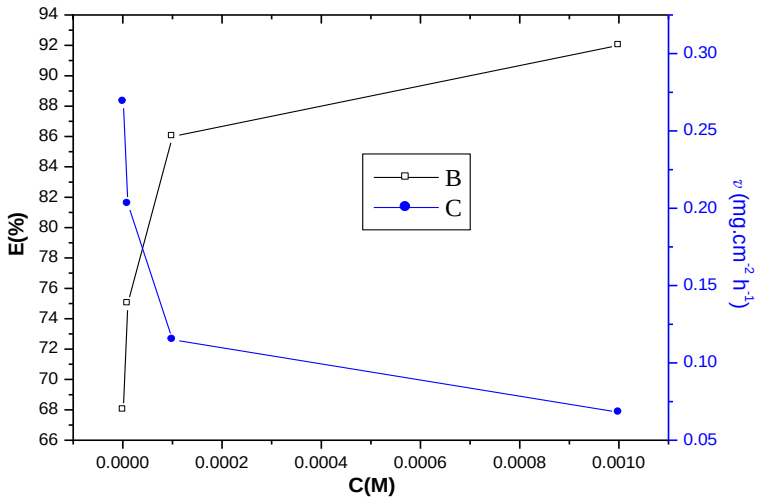

Figure 2. Variation of inhibition efficiency (E %) (B) and corrosion rate (v) (C) with the G3 inhibitor concentration at 308 K.

If it is assumed, that adsorption of the organic molecules or ions on the metal surface is the cause for the inhibitor action in acidic medium (1.0 M HCl) solution, then the surface coverage (θ) can be estimated from the inhibitor efficiency of θ = E(%)/100, if one assumes that the values of E(%) do not differ substantially from surface coverage [27]. An attempt was made to find a suitable adsorption isotherm, which can describe the concentration dependence of the inhibitor efficiency. Adsorption isotherms were determined, using the data of the gravimetric measurements, which are collected in a time interval of 6 hrs, considered sufficient for

adsorption equilibrium to be achieved [28-29]. Several adsorption isotherms (Langmuir, Temkin, Frumkin…) were assessed and the Langmuir adsorption isotherm was found to fit well with the experimental data obtained for G3. The Langmuir isotherm is given by the following equation [30]:

$$\frac{C_{inh}}{\theta} = \frac{1}{K_{ads}} + C_{inh} \qquad \textbf{(13)}$$

Where, θ is the fractional surface coverage; C_{inh} is the inhibitor concentration; and K_{ads} is the equilibrium constant of the adsorption process. K_{ads} is related to the standard Gibbs free energy of adsorption, $\Delta G°_{ads}$, according to [31]:

$$\Delta G_{ads} = -RT.ln(55{,}5.K) \qquad \textbf{(14)}$$

Where, R is the universal gas constant and T is the absolute temperature. The value 55.55 in the above equation is the concentration of water in solution in mol/l. Figure 3 showed the dependence of C_{inh}/θ against C_{inh}.

To calculate the adsorption parameters, the straight line was drawn using the least squares method. The experimental (points) and calculated isotherms (lines) were plotted in Figure3. A very good fit was observed with the regression coefficient up to 0.99 and the obtained line had slope very close to unity, which suggests that the experimental data are well described by Langmuir isotherm and exhibit single-layer adsorption characteristics. This kind of isotherm involves the assumption of no interaction between the adsorbed species on the electrode surface [32].

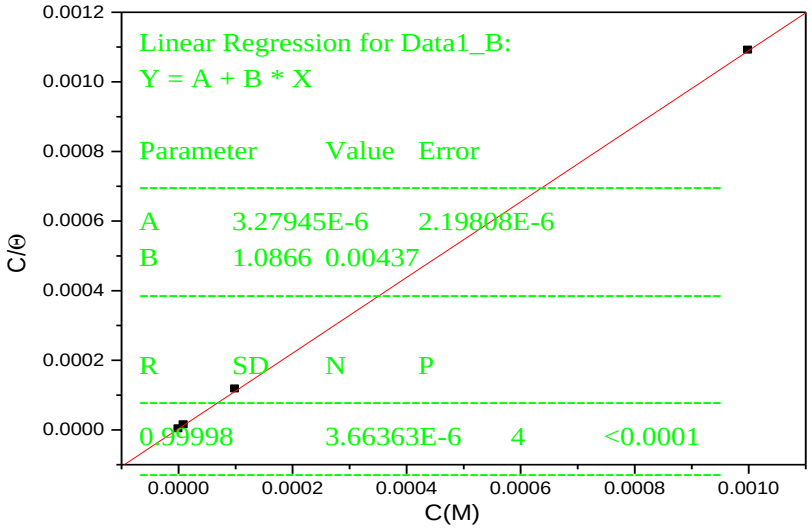

Figure 3. Langmuir adsorption of G3 on the mild steel surface in 1.0 M HCl solution at 308 K.

3.2. Electrochemical measurements

The electrochemical measurements were carried out using Volta lab (Tacussel - Radiometer PGZ 100) potentiostat controlled by Tacussel corrosion analysis software model (Voltamaster 4) at static condition. The corrosion cell used had three electrodes. The reference electrode was a saturated calomel electrode (SCE). A platinum electrode was used as auxiliary electrode of surface area of 1 cm^2. The working electrode was mild steel of the surface 1cm^2. All potentials given in this study were referred to this reference electrode. The working electrode was immersed in the test solution for 30 minutes to establish a steady state open circuit potential (E_{ocp}). After measuring the E_{ocp}, the electrochemical measurements were performed. All electrochemical tests have been performed in aerated solutions at 308 K. The EIS experiments were conducted in the frequency range with high limit of 100 kHz and different low limit 0.1 Hz at open circuit potential, with 10 points per decade, at the rest potential, after 30 min of acid immersion, by applying 10 mV as voltage peak-to-peak. Nyquist plots were made from these experiments. The best semicircle can be fit through the data points in the Nyquist plot using a non-linear least square fit so that it gives the intersection with the x-axis.

3.2.1. Electrochemical impedance spectroscopy (EIS)

The Nyquist plots of mild steel recorded after 30 minutes immersion in 1.0 M HCl solution in the absence and presence of different concentration of G3 inhibitor are shown in Figure 4. The parameters obtained from the Nyquist plots are listed in Table 1. In addition the obtained results can be interpreted using the equivalent circuit

presented in Figure 5, which has been used previously to model the steel/acid solution interface [33]. It is apparent from these plots that the obtained impedance was composed of one capacitive loop which its diameter was significantly changed after inhibitor addition and the greatest effect was observed at 10^{-3} M of G3. In addition, these impedance diagrams are not perfect semicircles and this difference has been attributed to frequency dispersion [34]. The addition of inhibitor is found to enhance R_{ct} values and bring down C_{dl} values. These observations clearly bring out the fact that the mild steel corrosion in 1.0 M HCl solution is controlled by a charge transfer process and the corrosion inhibition occurs through the adsorption of the G3 inhibitor on mild steel surface. The decrease in the C_{dl} values can result from the decrease in local dielectric constant and/or the increase in current density. The thickness of the electrical double layer, suggested that the G3 molecules function by adsorption at the metal/solution interface [35-37].

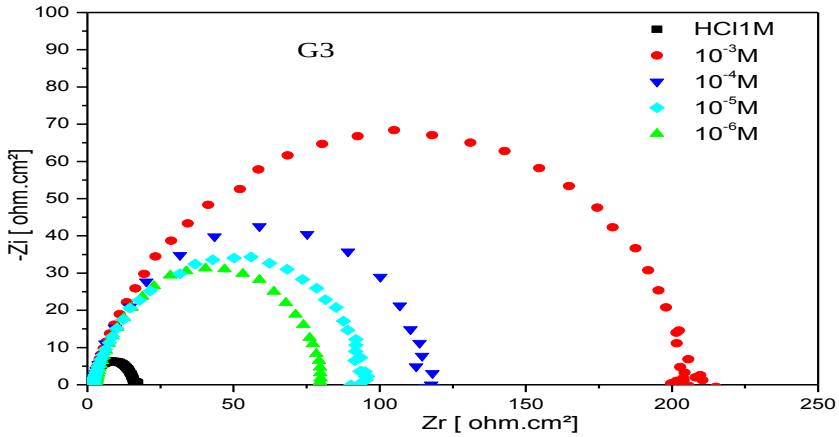

Figure 4. Nyquist plots of mild steel corrosion in 1.0 M HCl without and with different concentrations of G3 at open circuit potential. Symbols: Experimental data; Lines: Fitting data.

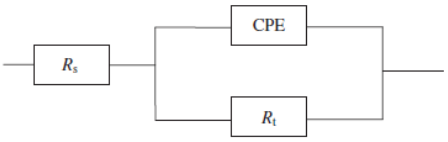

Figure 5. Electrochemical equivalent circuit used to fit the impedance measurements.

Table 1. Impedance parameters and inhibition efficiency values for mild steel after 1/2 h immersion period in 1 M HCl containing different concentrations of (G3) at 308 K.

Inhibitor	**Concentration of Inhibitor** (M)	$\mathbf{R_t}$ ($\Omega.cm^2$)	$\mathbf{C_{dl}}$ ($\mu F.cm^{-2}$)	$\mathbf{E_{Rt}}$ (%)
1.0 M HCl	-	17	200	--
G3	$\mathbf{10^{-6}}$	76	74	78
	$\mathbf{10^{-5}}$	90	52	81
	$\mathbf{10^{-4}}$	120	48	86
	$\mathbf{10^{-3}}$	205	35	**92**

3.2.2. Tafel Polarization Study

The potentiodynamic polarization curves of mild steel in 1.0 M HCl in the absence and presence of different concentrations of G3 are shown in Figure 6. Their electrochemical parameters are given in Table 2. These results show that G3 brings down (I_{corr}) value at all concentrations and the minimum values was obtained at 10^{-3} M. Moreover, it is noted that this compound causes a significant shift in (E_{corr}) values to cathodic values with a decrease in the current densities values indicating that it is a cathodic type inhibitor in 1.0 M HCl. It is noted that the cathodic and anodic Tafel slopes (βa and βc) change with the change in inhibitor concentration, indicating a change in the mild steel (iron) dissolution and hydrogen evolution oxidation-reduction reactions.

The data in Table 2 indicate that the values of I_{corr} decreased while the inhibition efficiency values increased in presence of inhibitor G3, which is due to the adsorption of inhibitor molecules on the mild steel surface [38-40].

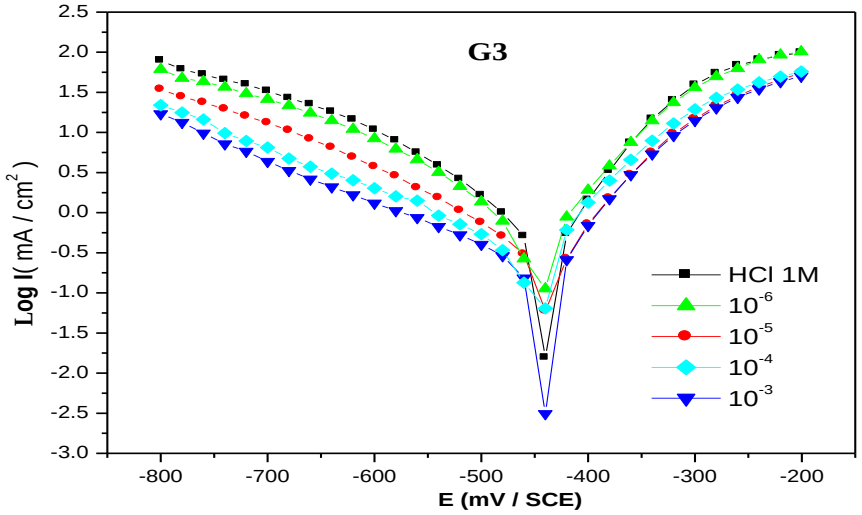

Figure 6. Potentiodynamic polarization curves for mild steel in 1.0 M HCl solutions without and with different concentrations of G3 at 308 K

Table 2. Potentiodynamic polarization parameters for the corrosion of mild steel in 1.0 M HCl solutions containing different concentrations of G3 at 308 K.

Inhibitor	**Concentration of Inhibitor** (M)	**E_{corr} (mV*vs.*SCE)**	**I_{corr} (µA/cm^2)**	**-βc (mV/dec)**	**βa (mV/dec)**	**E_p (%)**
1.0 M HCl	--	-450	1381	140	185	--
G3	**10^{-6}**	-455	532	107	125	61
	10^{-5}	-444	397	143	115	71
	10^{-4}	-456	209	111	89	85
	10^{-3}	-447	143	94	77	**90**

3.3. Quantum chemical calculations

The FMOs (HOMO and LUMO) are very important for describing chemical reactivity. The HOMO containing electrons, represents the ability (E_{HOMO}) to donate an electron, whereas, LUMO haven't electrons, as an electron acceptor represents the ability (E_{LUMO}) to obtain an electron. The energy gap between HOMO and LUMO determines the kinetic stability, chemical reactivity, optical polarizability and chemical hardness–softness of a compound [41]. Firstly, in this paper, we calculated the HOMO and LUMO orbital energies by using B3LYP method with 6-31G(d,p). All other calculations were performed using the results with some assumptions. The higher values of E_{HOMO} indicate an increase for the electron donor and this means a better inhibitory activity with increasing adsorption of the inhibitor on a metal surface, whereas E_{LUMO} indicates the ability to accept electron of the molecule. The adsorption ability of the inhibitor to the metal surface increases with increasing of E_{HOMO} and decreasing of E_{LUMO}. The HOMO and LUMO orbital energies and image of G3 were performed and were shown in Table 3 and Figure 7. High ionization energy (I= 6.83 eV, I= 6.78 eV in the gaseous and aqueous phases, respectively) indicates high stability [42]. The number of electrons transferred (ΔN) was also calculated and tabulated in Table 3. The obtained ΔN value (0.53 < 3.6), indicates that the tendency of the G3 molecule to donate electrons to the metal surface is so high [43-44].

For a system of N electrons, independent single-point calculations were made for corresponding N+1 and N-1 electron systems. The resulting natural population analysis yields to P k (N-1), P k (N), and P k (N+1), the population for all atoms k [45, 46]. In a finite-difference approximation from Mulliken population analysis of atoms in molecules, depending on the direction of the electron transfer, then the condensed Fukui functions were computed using the following equations from the Exact Theory [47].

To get some insight into the local reactivity of the studied inhibitors, the Fukui functions were computed since they are the relevant reactivity indicators in the electron-transfer controlled reactions such as corrosion

inhibition process [47, 48]. Their values are used to identify which atoms in the inhibitor are more prone to undergo an electrophilic or a nucleophilic attack. The calculated values of the f_k^+ for all inhibitors are mostly localized on the benzothiazine ring. Namely *S_{12}*, *O_{13}*, *C_{21}*, *C_{25}*, *H_{28}* and *Cl_{29}*, indicating that the benzothiazine ring will probably be the favorite site for nucleophilic attacks [49-50]. The results also show that S_{12} atom is suitable site to undergo both nucleophilic and electrophilic attacks, probably allowing them to adsorb easily and strongly on the mild steel surface.

Table 3. Quantum chemical descriptors of the studied inhibitor G3 at B3LYP/6-31 G** in gaseous (G) and aqueous (A) phases.

Inhibitor	Phase	*TE* (**eV**)	E_{HOMO} (**eV**)	E_{LUMO} (**eV**)	Gap *ΔE* (**eV**)	*μ* (**D**)	IP (**eV**)	EA (**eV**)	*X* (**eV**)	*η* (**eV**)	*ω*	*σ*	*Δ*N
G3	**G**	-42611.1	-6.8262	-0.1744	6.6518	3.5183	6.8262	0.1744	3.5003	3.3259	1.8419	3.3259	0.5261
	A	-42611.3	-6.7832	-0.0419	6.7413	4.7036	6.7832	0.0419	3.4125	3.3706	1.7275	3.2967	0.5322

Table 4. Pertinent natural populations and Fukui functions of **G3** calculated at B3LYP/6-31G in gaseous (G) and aqueous (A) phases.

Atom k	Phase	P(N)	P(N-1)	P(N+1)	f_k^-	f_k^+	f_k^0
S_{12}	G	15,15808	15,63948	15,40974	0,4814	15,1581	0,1149
	A	15,14886	15,66227	15,36084	0,5134	-0,2120	0,1507
O_{13}	G	8,60321	8,67548	8,5601	0,0723	0,0431	0,0577
	A	8,68455	8,71431	8,60817	0,0298	0,0764	0,0531
C_{21}	G	6,04473	6,13189	5,98498	0,0872	0,0598	0,0735
	A	6,05076	6,12907	5,99491	0,0783	0,0559	0,0671
C_{25}	G	6,10131	6,28623	6,10761	0,1849	-0,0063	0,0893
	A	6,11407	6,31637	6,09167	0,2023	0,0224	0,1124
H_{28}	G	0,49406	0,58499	0,53631	0,0909	-0,0423	0,0243
	A	0,48132	0,56557	0,52664	0,0843	-0,0453	0,0195
Cl_{29}	G	16,99816	17,06269	16,90618	0,0645	0,0920	0,0783
	A	17,0113	17,06024	16,96783	0,0489	0,0435	0,0462

The final optimized geometries of **G3** in gaseous and aqueous phases, selected valence bond angle, dihedral angles and bond lengths are given in Figure 7.

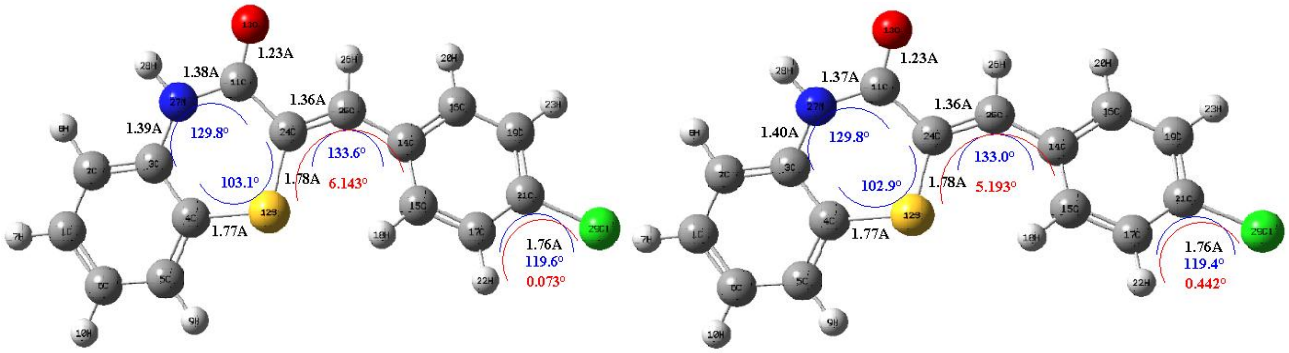

G3 Gas phase **G3** Aqueous phase

Figure 7. Optimized molecular structures, selected dihedral angles (red), valence bond angle (blue) and bond lengths (black) of the studied G3 inhibitor calculated in gaseous and aqueous phases at B3LYP/6-31G(d,p) level. The analysis of the theoretical results, indicate that the molecular structure of **G3** inhibitor is non-planar.

Table 5. The HOMO and the LUMO electrons density distributions of the studied G3 inhibitor computed at B3LYP/6-31G (d,p) level in gaseous and aqueous phases.

	G3 Gaseous phase	**G3** Aqueous phase
HOMO	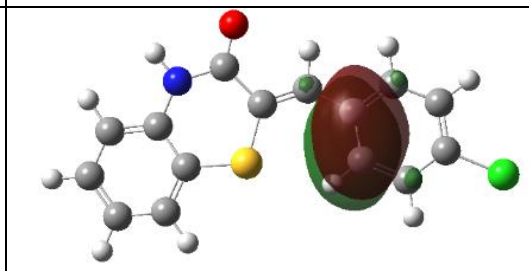	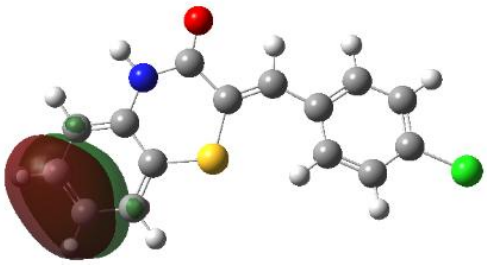
LUMO	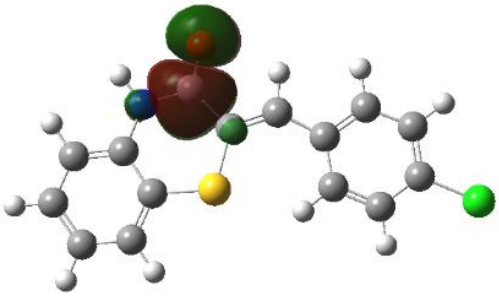	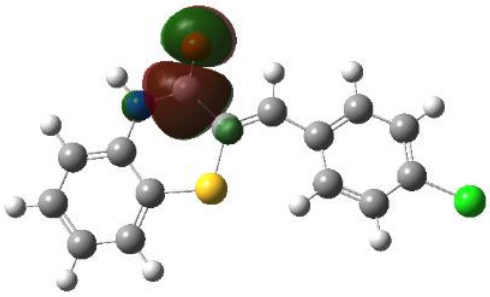

The inhibition efficiency afforded by **G3** may be attributed to the presence of the lone pair of electrons on O.

Conclusion

The following conclusions may be drawn from the study:

- The inhibition efficiency of (G3) for mild steel in 1.0 M HCl solution increases with increasing its concentration.
- The corrosion current density significantly decreases and corrosion potential slightly changes with the addition of G3 in HCl solution, and the synthesized inhibitor of G3 is cathodic type inhibitor.
- The adsorption of G3 on the mild steel surface obeys Langmuir isotherm.
- The presence of G3 in 1.0 M HCl solution increases charge transfer resistance, while it reduces double layer capacitance values. This result can be attributed to the increase of electrical double layers thickness.
- The large efficiency of G3 inhibitor is due to the presence of many oxygen atoms in this (2Z)-(4-chlorobenzylidene)-2*H*-[1,4]-benzothiazin-3(4*H*)-one (**G3**). The calculated quantum chemical parameters such as HOMO-LUMO gap, E_{HOMO}, E_{LUMO}, dipole moment (μ) and total energy (TE) were found to give reasonably good correlation with the efficiency of the corrosion inhibition.

References

1.Chadli R., Elazouzi M., Khelladi I., Elhourri A.M., Elmsellem H., Aouniti A., Kajima Mulengi J., Hammouti B., *Portugaliae Electrochimica Acta.* 35 (2017) 65-80.

2. Elmsellem H., Harit T., Aouniti A., Malek F., Riahi A., Chetouani A., and Hammouti B., *Protection of Metals and Physical Chemistry of Surfaces*. 51 (2015) 873–884.

3. Aziate G., El Yadini A., Saufi H., Benhmama A., Harhar H.,Gharby S., El Hajjaji S., *J. Mater. Environ. Sci.* 6(7)(2015) 1877-1884.

4. Ezznaydy G., Shaban A., Telegdi J., Ouaki B., El Hajjaji S., *J. Mater. Environ. Sci*. (7)(2015) 1819-1823.

5. Sebbar N.K., Mekhzoum M.E.M., Essassi E.M., Zerzouf A., Talbaoui A., Bakri Y., Saadi M., Ammari L.E., *Res. Chem. Intermed*., 42(9) (2016) 6845–6862.
6. Sebbar N. K., Ellouz M., Zerzouf A. & Essassi E. M., *J. Mar. Chim. Heterocycl*. 14(1) (2015) 56-62.
7. Sebbar N.K., Mekhzoum M. E. M., Essassi E. M., Abdelfettah Z., OuzidanY., KandriRodi Y., Talbaoui A. Bakri Y., *J.Mar.Chim.Heterocycl*. 15(1) (2016)1-11.
8. Sebbar, N. K., Ellouz, M., Essassi, E. M., Saadi, M. & El Ammari, L. *Acta Cryst*. E71 (2015) o423–o424.
9. Sebbar, N. K., Ellouz, M., Essassi, E. M., Saadi, M. & El Ammari, L. *IUCr Data*. (2016). 1, x161012.
10. Trapani G., Reho A., Morlacchi F., Latrofa A.,Marchini P., Venturi F., Cantalamessa F., *Farmaco. Ed. Sci.* 40(5) (1985)369.
11. Park M. S., Chang E. S., Lee M. S., Kwon S. K., *Bull. Korean Chem. Soc*., 23(12) (2002)1836.
12. Wammack R., Remzi M., Seitz C., Djavan B., Marberger. M., *Eur. Urol*., 41(6) (2002) 596.
13. Laban G., Guenther W., Lohmann D., *Ger. Patent DD*., 247674 (1987).
14. Pijak M. R., Turcani P., Turcaniova Z., Buran I., Gogolak I., Mihal A., Gazdik F., *Bratisl. Med. J*. 103(12) (2002) 467-469.
15. Zia-ur-Rehman M., Choudary J. A., Elsegood M. R. J., Siddiqui H. L., Khan K. M., *Eur. J. Med. Chem*., 44(3) (2009) 1311.
16. Niewiadomy A., Matysiak J., Karpinska M. M., *Archiv. Pharm*., 344 (2011) 224–230.
17. Gautam N., Ajmera N., Gupta S., Gautam D.C., *Eur. J. Chem*., 3 (2012)106–111.
18. Hjouji M. Y., Djedid M., Elmsellem H., Kandri Rodi Y., Ouzidan Y., Ouazzani Chahdi F., Sebbar N. K., Essassi E. M., Abdel-Rahman I., Hammouti B., *J. Mater. Environ. Sci*.7(4)(2016)1425-1435.
19. Sikine M., Kandri Rodi Y., Elmsellem H., Krim O., Steli H., Ouzidan Y., Kandri Rodi A., Ouazzani Chahdi F., Sebbar N. K., Essassi E. M., *J. Mater. Environ. Sci*, 7 (4) (2016) 1386-1395.
20. Chakib I., Elmsellem H., Sebbar N. K., Lahmidi S., Nadeem A., Essassi E. M., Ouzidan Y., Abdel-Rahman I., Bentiss F., Hammouti B., *J. Mater. Environ. Sci*. 7(6) (2016) 1866-1881.
21. Elmsellem H., Basbas N., Chetouani A., Aouniti A., Radi S., Messali M., Hammouti B., *Portugaliae. Electrochimica. Acta*. 2 (2014) 77.
22. Selwood D. L., Brummell D. G., Budworth J., Burtin G. E., Campbell R. O., Chana S. S., Charles I. G., Fernandez P. A., Glen R. C., Goggin M. C., Hobbs A.J., Kling M. R., Liu Q., Madge D. J., Meillerais S., Powell K. L., Reynolds K., Spacey G. D., Stables J. N., Tatlock M. A., Wheeler K. A., Wishart G., Woo C.K., *J. Med. Chem.* 44 (2001)78.
23. Pearson R.G., *Inorg. Chem*. 27 (1988) 734.
24. Sastri V.S., Perumareddi J.R., *Corrosion*. 53 (1997) 617.
25. Saufi H., El Yadini A., Eddaif L., Harhar H., Gharby S., El Hajjaji S. *J. Mater. Environ. Sci.* 6 (7) (2015) 1845-1849.
26. Udhayakala P., Rajendiran T. V., Gunasekaran S., *Journal of Chemical, Biological and Physical Sciences* A, 2(3) (2012)1151–1165.
27. El Ouadi Y. , Manssouri M., Bouyanzer A., Majidi L., Bendaif H., Elmsellem H., Shariati M.A., Melhaoui A., Hammouti B., *Microbial Pathogenesis* .107 (2017) 1-6.
28. Tribak Z., Kandri Rodi Y., Elmsellem H., Abdel-Rahman I., Haoudi A., Skalli M. K., Kadmi Y., Hammouti B., Ali Shariati M., Essassi E. M., *J. Mater. Environ. Sci*. 8 (2017) 1116 -1127.
29. Filali Baba Y., Elmsellem H., KandriRodi Y., Steli H., Ouzidan Y., Ouazzani Chahdi F., Sebbar N. K., Essassi E. M., Hammouti B., *Der Pharma Chemica*. 8(4)(2016)159-169.
30. Hjouji M. Y., Djedid M., Elmsellem H., Kandri Rodi Y., Benalia M., Steli H., Ouzidan Y., Ouazzani Chahdi F., Essassi E. M., Hammouti B., *Der Pharma Chemica*. 8(4)(2016)85-95.
31. Elmsellem H., Nacer H., Halaimia F., Aouniti A., Lakehal I., Chetouani A., Al-Deyab S. S., Warad I., Touzani R., Hammouti B, *Int. J. Electrochem. Sci*. 9 (2014) 5328.
32. Elmsellem H., Aouniti A., Toubi Y., Steli H., Elazzouzi M., Radi S., Elmahi B., El Ouadi Y., Chetouani A., Hammouti B., *Der Pharma Chemica*.,7 (2015) 353-364.
33. Lahmidi S., Elmsellem H., Elyoussfi A., Sebbar N. K., Essassi E.M., Ouzidan Y., KandriRodi Y., DguiguiK., El Mahi B. and Hammouti B., *Der Pharma Chemica*. 8(1) (2016) 294.
34. Bendaha H., Elmsellem H., Aouniti A., Mimouni M., Chetouani A., Hammouti B., *Physicochemical Mechanics of Materials.* 1 (2016) 111-118.
35. Sen K.D., Jorgenson C., *Springer, Berlin*. 66 (1987).

36. Elmsellem H., Aouniti A., Khoutoul M., Chetouani A., Hammouti B., Benchat N., Touzani R. and Elazzouzi M., *J. Chem. Pharm. Res*. 6 (2014) 1216.
37. Elmsellem H., Karrouchi K., Aouniti A., Hammouti B., Radi S., Taoufik J., Ansar M., Dahmani M., Steli H. and El Mahi B., *Der Pharma Chemica*. 7(10) (2015)237-245.
38. Sebbar N. K., Elmsellem H., Boudalia M., lahmidi S., Belleaouchou A., Guenbour A., Essassi E. M., Steli H., Aouniti A., *J. Mater. Environ. Sci*. 6 (11) (2015) 3034-3044.
39. Govindarajan M., Karabacak M., *Spectrochim. Acta Part A Mol Biomol Spectrosc*. 85(2012) 251.
40. Elmsellem H., Elyoussfi A., Sebbar N. K., Dafali A., Cherrak K., Steli H., Essassi E. M., Aouniti A. and Hammouti B., *Maghr. J. Pure &Appl. Sci*.1 (2015) 1-10.
41. Govindarajan M., Karabacak M., *Spectrochim. Acta Part A Mol Biomol Spectrosc*. 85 (2012) 251.
42. Essaghouani A. L., Elmsellem H., Ellouz M., El Hafi M., Boulhaoua M., Sebbar N. K., Essassi E. M., Bouabdellaoui M., Aouniti A. and Hammouti B., *Der Pharma Chemica*. 8(2) (2016)297-305.
43. EL Aoufir Y., Lgaz H., Bourazmi H., Kerroum Y., Ramli Y., Guenbour A., Salghi R., El-Hajjaji F., Hammouti B., Oudda H., *J. Mater. Environ. Sci*. 7 (12) (2016) 4330-4347
44. Elyoussfi A., Dafali A., Elmsellem H., Steli H., Bouzian Y., Cherrak K., El Ouadi Y., Zarrouk A., Hammouti B., *J. Mater. Environ. Sci.* 7 (9) (2016) 3344.
45. Ramdani M., Elmsellem H., Elkhiati N., Haloui B., Aouniti A., Ramdani M., Ghazi Z., Chetouani A. and Hammouti B., *Der Pharma Chem.*7 (2015) 67-76.
46. Sikine M., Elmsellem H., KandriRodi Y., Steli H., Aouniti A., Hammouti B., Ouzidan Y., OuazzaniChahdi F., Bourass M., Essassi E.M., *J. Mater. Environ. Sci.* 7 (12) (2016) 4620-4632.
47. Quijano M.A., Pardav M.P., Cuán A., Romo M.R., Silva G.N., Bustamante R.Á., López A.R., Hernández H.H., *Int. J. Electrochem. Sci*. 6 (2011) 3729.
48. Becke A.D., *Phys. Rev. A*. 38 (1988) 3098.
49. Kumar S., Ladha D.G., Jha P.C., and Shah N.K., *International Journal of Corrosion Volume*. (2013), ID 819643, 10 http://dx.doi.org/10.1155/2013/819643.
50. Khaled K.F., *Applied Surface Science*, 256(22) (2010) 6753.